IEEJ Journal of Industry Applications, vol. 9, no. 3, pp. 1–10, 2020

Application of the IGCT for Resonant Conversion with Low Switching Losses

D. Stamenkovic and D. Dujic

POWER ELECTRONICS LABORATORY
ÉCOLE POLYTECHNIQUE FÉDÉRALE DE LAUSANNE

IEEJ Journal of Industry Applications
Vol.9 No.3 pp.1–10 DOI: 10.1541/ieejjia.9.1

Paper

Application of the IGCT for Resonant Conversion with Low Switching Losses

Dragan Stamenkovic[*a)] Non-member, Drazen Dujic[*] Non-member

(Manuscript received July 11, 2019, revised Nov. 28, 2019)

An LLC series resonant converter presents a viable opportunity for the realization of a DC solid-state transformer. As the DC-based power system increasingly garners the attention of academia and industry, the need for reliable, economical and efficient voltage transformation with galvanic isolation has emerged. The integrated gate-commutated thyristor (IGCT) is an attractive switch for such implementation because of its advantages over the insulated gate bipolar transistor, namely the lowest conduction losses in the class. This work shows that the IGCT can be easily implemented as a switching element in a resonant converter without the need for the protective clamping circuit. Resonant switching operation is demonstrated and supported by experimental data, and high efficiency is confirmed at high switching frequencies.

Keywords: IGCT, series resonant converter, LLC, DC-DC transformer, MVDC, solid state transformer, high power DC-DC

1. Introduction

DC-DC high power conversion in medium voltage applications posses significant challenges that are currently being addressed both in academia and industry. With the proliferation of High Voltage Direct Current (HVDC) transmission networks in recent times, natural question of converting the existing Alternating Current (AC) distribution networks to Direct Current (DC) distribution arises. Nowadays, HVDC transmission stops at a substation where it is converted to AC for further transmission and distribution, introducing the bulky 50/60 Hz equipment and components. Key missing elements for a full system transformation from AC to DC are reliable DC breakers for protection of the equipment during faults and DC transformers for efficient and reliable voltage transformation and galvanic insulation between different voltage levels.

The two topics, DC breaker and DC transformer are in the focus of worldwide research with more and more attention arising in industry through pilot projects and cooperation with academia [(1)–(3)]. Steady pace research shows the promising results in the area of increasing the power transfer capacities by conversion of existing power network to DC while lowering the footprint of the supporting substations by using more efficient power electronics equipment [(4)].

Significant results have already been presented regarding the HVDC to Medium Voltage Direct Current (MVDC) transformation with a Modular Multilevel Converter (MMC) at the heart of the solution [(5)]. Further distribution requires MVDC to MVDC and MVDC to Low Voltage Direct Current (LVDC) transformation as the system gets closer to the load. Practical implementation for larger system conversion is still far away but more specific and closed systems are already considering the DC as the backbone for the power transfer.

One of the most fertile grounds for the MVDC application is the marine sector [(6)–(8)], where the standards, defining preferred network topologies and voltage levels, are already available. Industry is supporting this paradigm change that offers efficient fuel utilization on the ship, lower count of equipment elements, smaller footprint and less weight. Another application of MVDC is found in high power wind and solar power plants [(4)(9)(10)], where DC collection offers the opportunity for unmatched power plant efficiency.

In the area of MVDC transformation, two variants of the high power DC-DC converter topologies are most commonly found and discussed in literature: Dual-Active Bridge (DAB) [(11)(12)] and LLC Series Resonant Converter (LLC-SRC) [(13)(14)]. Their respective half-bridge variants are presented in the Figs. 1(a) and (b). Even though DAB has one element less than the LLC-SRC, LLC-SRC is chosen for the further analysis because of the advantages that it offers over the DAB configuration:

- Quasi sinusoidal resonant tank currents
- Natural soft-switching of the semiconductors
- Absence of the need for tight regulation of the output voltage

In both topologies Insulated Gate Bipolar Transistor (IGBT) as a switching element is dominantly used. Being an industrial standard semiconductor switch of choice, it is available in various ratings and packages, optimized for different applications. Its alternative in the medium voltage power electronics can be found in the Integrated Gate-Commutated Thyristor (IGCT), another mature technology based on thyristor structure and optimized for high current applications [(15)–(18)].

IGCT, being exclusively a press-pack device, is meant for heavy duty applications and can easily find its role within the DC transformer world. Having the thyristor structure,

a) Correspondence to: Dragan Stamenkovic. E-mail: dragan.stamenkovic@epfl.ch
* École Polytechnique Fédérale de Lausanne
Station 11, Lausanne, Switzerland

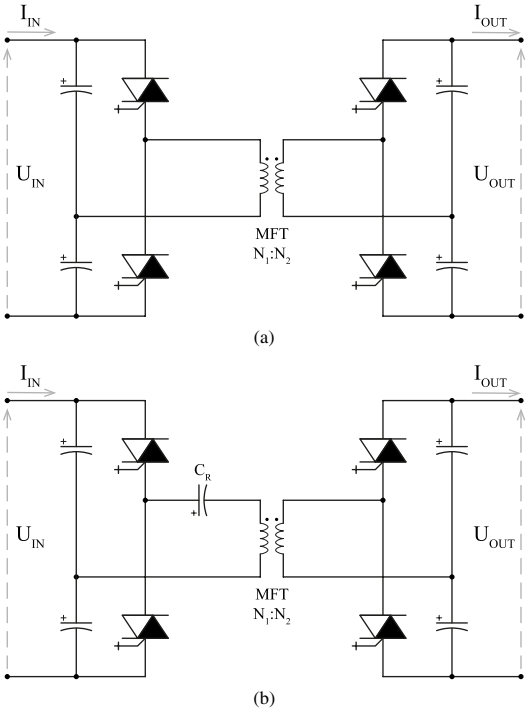

Fig. 1. Two popular isolated DC-DC converter topologies with an RC-IGCT as a switching element a) dual-active bridge b) series resonant converter

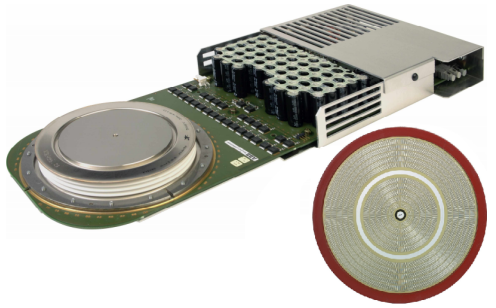

(a)

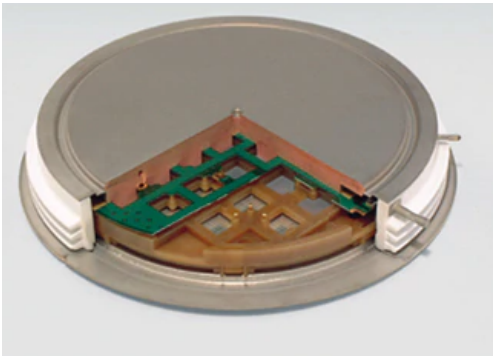

(b)

Fig. 2. a) IGCT wafer constuction [21] b) Internal construction of the press-pack IGBT [22]

it is advantageous over the IGBT regarding the conduction losses [19][20]. From the point of switching energy losses, turn-on losses of the IGCT are negligible and omitted from the datasheets, while the turn-off losses are relatively similar to those of IGBT. It should be noted here that IGCT's rate of current change during turn-on cannot be controlled through the gate as in case of the IGBT but only through addition of an external inductor for this purpose. In the hard switching applications, IGCT is always accompanied by the clamp circuit (shown in Fig. 4 and discussed in more details later in the paper) that protects the free-wheeling diodes against excessive di/dt at IGCT's turn-on and since the clamping inductor takes over the full DC-link voltage, IGCT turns on with practically zero voltage at its power terminals. As a consequence, turn-on losses are negligible.

Looking at the physical properties of the IGCT, Fig. 2(a), it is noticed that it is made of one circular wafer with GCT fingers evenly distributed over the surface of the device. Press-pack IGBT device cannot be made in this way but instead, a number of rectangular dies are spread over the circular surface of the package, Fig. 2(b), which is disadvantageous in terms of thermal contact to the case when compared to the IGCT. This is the reason why, for the same package size, $R_{th(j-c)}$ is usually lower for the IGCT.

Having all the advantages in mind, it would be beneficial to test the applicability of the IGCT in the LLC-SRC configuration. This type of DC transformer offers an opportunity of a bulk power transfer, medium frequency operation, galvanic isolation between input and output and increased reliability.

The main contributions of this paper are related to implementation of the IGCT switching device in the LLC-SRC topology for the DC transformer implementation together with the technical challenges for such an application and experimental data to support the claims. Required design parameters, such as turn-off delay time t_{DOFF} and turn-off energy losses E_{off}, are identified and their design importance explained. The parameters are experimentally obtained and later used for demonstration of the continuous operation in LLC-SRC mode. Switching of the IGCT without the clamping circuit is also demonstrated and validity of the IGCT resonant operation proved.

Paper is structured in a way that Section 2 presents the basic LLC-SRC operation and the requirements for the safe operation of the IGCT based half-bridge. Basic clamp circuit role and operation in hard-switching applications is described in Section 3, providing the explanation why is the the clamp circuit not necessary in the LLC-SRC application. Section 4 introduces laboratory test setup, designed and assembled for the testing purposes of the IGCT switches. The biggest portion of the paper is taken by the Section 5, which contains the experimental results and discussion regarding the resonant pulse testing in Subsection 5.1, and continuous resonant operation in Subsection 5.2. Conclusions are presented in Section 6.

2. LLC Series Resonant Converter

Basic circuit for LLC-SRC analysis is presented in Fig. 3(a). Resonant capacitor C_R is in series connection with resonant inductor L_R which can be implemented as a discrete component or integrated into the leakage inductance of the Medium Frequency Transformer (MFT). Magnetizing inductor L_M is connected in parallel to the MFT and simulates its magnetization inductance. Input half-bridge is realized using a series connection of two Reverse Conducting IGCTs (RC-IGCTs), S_1 and S_2, while the output half-bridge consists of two diodes, D_1 and D_2. Such a configurations allows for the

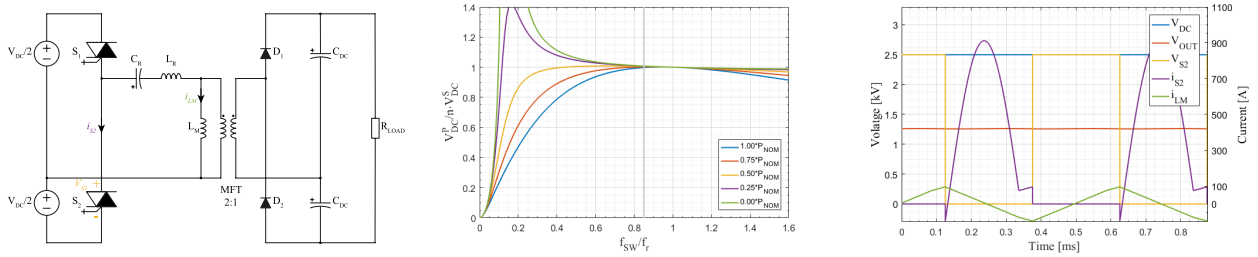

(a) (b) (c)

Fig. 3. a) Half-bridge LLC-SRC b) LLC-SRC transfer characteristic c) LLC-SRC characteristic voltage and current waveforms

unidirectional flow of energy; if a bidirectional flow is required, the output half-bridge diodes can be replaced by two RC-IGCTs. RC-IGCT is the semiconductor switch having the anti-parallel diode integrated on the same wafer with the IGCT, all in one press-pack type of package.

LLC-SRC in the Fig. 3(a) operates with the switching frequency lower than its resonant frequency. This kind of operation allows the IGCT to turn-off at the same value of the turn-off current, regardless of the load. Constant turn-off current is essential requirement for keeping the turn-off energy losses at minimum throughout the operation of the converter.

Switching frequency is lower but close in value to the resonant frequency, in order to keep the output voltage of the converter stiff for wide range of load without implementing any control action. Typical load dependent transfer characteristics of the LLC-SRC are shown in Fig. 3(b), where a range of negligible output voltage variations (load independent operation) can be identified in the near vicinity of a resonant frequency. Normalized transfer characteristics in Fig. 3(b) are obtained using the first harmonic approximation method, described in [23] and applied for the circuit in Fig. 3(a).

Figure 3(c) shows some typical current and voltage waveforms during the normal operation of the LLC-SRC and from the same figure, zero-voltage turn-on can be identified. Electrical current of the resonant tank is the sum of the magnetizing current of the MFT and resonant current. Switching frequency being lower than resonant makes the current in the resonant tank, right before the S_1 is turned off, equal to the magnetizing current of the MFT. S_1 is conducting this current and after the S_1 turns off, current is immediately commutated to the anti-parallel diode of the S_2 with its IGCT still in the off-state. Turning off of the S_1 reverses the polarity at the input of the resonant circuit, triggering a new resonant half-cycle in the circuit. Sum of the resonant and magnetization current now flows through the anti-parallel diode of S_2, producing a low voltage drop across the IGCT, reverse biasing it. This current is the negative part of the S_2 current in Fig. 3(c). For the successful zero-voltage turn-on of the S_2 IGCT, a turn-on pulse should be released during the period of its diode conduction. IGCT is then ready to take over the resonant tank current and does so at practically zero voltage drop at its terminals because the resonant tank current crosses zero at this point, making the voltage drop of its anti-parallel diode practically zero.

Turn-off of the S_1 at the above instant is a hard turn-off and by tailoring the magnetizing inductance of the MFT, the value of the turn-off current can be defined and kept constant throughout the LLC-SRC operation (turn-off current is load independent). Turn-off energy losses are directly proportional to the value of the turn-off current and can be kept at minimum by choosing the lowest possible turn-off current for the design, which does not compromise soft-switching during turn-on. On the other hand, the duration of the turn-off process of the IGCT is inversely proportional to the turn-off current and prolongs as the current drops. Knowledge of the turn-off duration is essential for the proper selection of the required dead-time - t_D. Manufacturer's datasheet defines the parameter t_{DOFF}, turn-off delay time, as the period between moment of optical signal at the input of the IGCT's gate driver going low and moment when the anode current falls to 40% of the starting value. It is usually given as one number for the worst case hard-switching scenario.

Having the described limitations in mind, dead-time requirement can be expressed as:

$$t_{DOFF} < t_D < t_{DCND} \cdots\cdots\cdots\cdots\cdots\cdots\cdots\cdots\cdots\cdots (1)$$

where t_{DOFF} is turn-off delay time and t_{DCND} is the anti-parallel diode conduction time (negative current period in Fig. 3(c)). Diode conduction time can be evaluated from the expression of electrical current flowing through the switch during this period and is a sum of resonant tank and magnetizing current:

$$i_S(t) = I_{rm} \sin(\omega_r t) + 4 I_{off} f_{sw} t - I_{off} \cdots\cdots\cdots\cdots (2)$$

under the condition that:

$$i_S(t_{DCND}) = 0 \cdots\cdots\cdots\cdots\cdots\cdots\cdots\cdots\cdots\cdots (3)$$

Given Eq. (3) does not have an analytical solution and numerical methods can be used in its evaluation. First order approximation will be used here and the approximate expression for the diode conduction time is given by the Eq. (4), where I_{off} is the IGCT turn-off current, I_{rm} is the amplitude of the resonant current, f_{sw} and f_r switching and resonant frequency respectively.

$$t_{DCND} = \frac{I_{off}}{4 I_{off} f_{sw} + 2\pi I_{rm} f_r} \cdots\cdots\cdots\cdots\cdots\cdots (4)$$

Dependency of the turn-off delay time with the turn-off current is not available in the IGCT datasheet and is evaluated experimentally. Results are shown further in the paper.

3. IGCT Clamp Circuit

As mentioned earlier, hard-switching application of IGCT

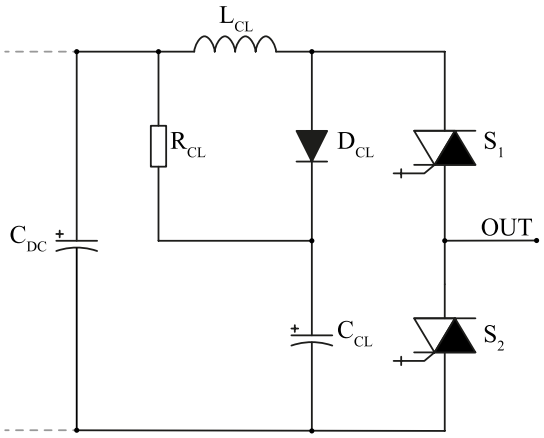

Fig. 4. IGCT Half-bridge with a clamp circuit

involves the usage of the clamp circuit as shown in the Fig. 4. Rate of change of the current when the S_1 turns on cannot be controlled the means of gate driver resistance as in IGBT, but, for IGCT, it is limited only by the external circuit parameters. At the turn-on moment of S_1, anti-parallel diode of S_2 turns off (positive output current assumed) and as it cannot withstand infinite di/dt at turn-off, an external inductor L_{CL} is added between the DC-link and the half-bridge to limit the di/dt to the acceptable level.

The rest of the clamp circuit elements are there to help with the turn-off of S_1. Absence of these would cause fatal overvoltage spike at IGCT's terminals since L_{CL} is relatively high, discrete inductance added in the circuit. After the current commutates from S_1 to S_2, magnetic energy accumulated in the clamp inductor transfers to the clamp capacitor, charging it to the voltage level higher than the DC-link but still within safe operation limits of the switch. Resistor R_{CL} enables discharge of clamp capacitor's, C_{CL}, electric energy back to the DC-link, recuperating a part of the magnetic energy stored in the L_{CL}. The process is symmetrical for the switch S_2.

Additional positive impact of the L_{CL} is that it enables zero voltage turn-on of the IGCT by taking over the full DC-link voltage until the switch takes over the current. This way the turn-on energy losses of the IGCT become practically zero. L_{CL} plays an important role in the case of the short circuit of the at the output of the converter bridge, limiting the short circuit current and its rate of change, providing more time for the protection to react.

Provided that the main role of the L_{CL} is to limit di/dt for the anti-parallel diodes, question arises if this inductor is necessary in the case of LLC-SRC. Figure 3(c), showing the typical current stress of the switches during the normal operation, suggests a low di/dt stress on the diodes at their turn-off. The value for the rate of change of current can be estimated by differentiating Eq. (2) and finding its maximum, which is at moment $t = 0$ - right after the current is commutated from the IGCT.

$$\left.\frac{di}{dt}\right|_{max} = 2\pi I_{rm} f_r + 4 I_{off} f_{sw} \cdots\cdots\cdots\cdots\cdots\cdots\cdots\cdots (5)$$

For the example waveforms presented in Fig. 3(c), the maximum diode di/dt is 14 A/μs, which is the order of magnitude lower than the requirement found in the datasheet of the device used in the test setup (285 A/μs max di/dt). This is

Fig. 5. Multifunctional laboratory test setup

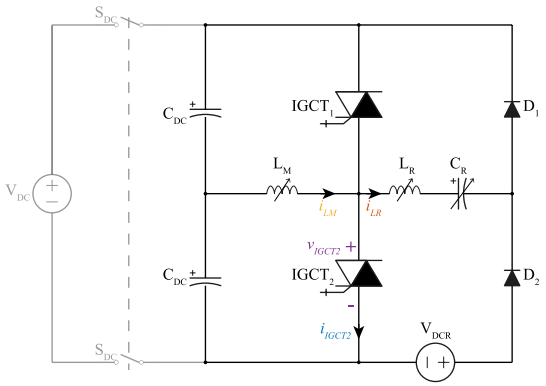

Fig. 6. Connection diagram of the test setup when used resonant pulse and continuous resonant operation tests

the huge margin for the variation of resonant/switching frequency, as well as the turn-off and the maximum resonant current, practically ensuring the clamp-less operation of the IGCT bridge.

4. Test Setup

In order to test the behavior of the IGCT switches under the resonant operating conditions, dedicated test setup was designed and built. Fig. 5 shows the multifunctional laboratory test setup used to perform the double pulse, resonant pulse and continuous operation tests on the IGCT switching devices. Connection diagram used for the resonant pulse test as well as for continuous resonant operation test is shown in the Fig. 6. The water cooled IGCT stack is used for the implementation of the switching half-bridge with an external water circulation unit keeping the fluid within the safe temperature margins. Basic information about RC-IGCT used in the test setup is given in Table 1.

Variable magnetization inductance L_M is simulating the magnetization current of the MFT and can be discretely varied in order to set the predefined turn-off current of interest for the RC-IGCTs in the half-bridge. Resonant tank is also

Table 1. Semiconductor devices used in the test setup

	IGCT	Reverse Diode
Manufacturer	ABB	ABB
Model	5SHX 1445H	5SHX 1445H
Forward blocking voltage	5500 V	5500 V
V_{DC}	3300 V	-
I_{TGQM}	900 A	-
I_{FAVM}	-	170 A
Threshold Voltage V_{T0}, V_{F0}	1.65 V	2.53 V
Slope Resistance r_T, r_F	2 mΩ	4.3 mΩ

variable so that its frequency can be varied in a discrete manner, depending on the test requirements. L_R and C_R are variable discrete components that can be combined to obtain the resonant frequency of interest and the diodes D_1 and D_2 provide a return path for the resonant current back through the RC-IGCT.

High voltage source, V_{DC} is used to charge the DC-link, providing the working voltage stress for the switching RC-IGCTs and can go up to the 5 kV. Being a low current source it only provides the energy losses in the magnetizing inductor and the turn-off losses of the RC-IGCTs. On the other hand, high current source, V_{DCR}, is used to ensure the current stress for the switches, covering conduction energy losses in the RC-IGCTs, the resonant tank and returning diodes.

This way, flexible current and voltage stress for the IGCTs under test is achieved without having a full LLC-SRC that would require two separate MVDC networks to circulate the power. Energy taken for the sources is used to cover only the losses in the test circuit which makes the power consumption of the setup relatively low.

Based on discussion provided in previous section, it should be noted that the clamp circuit was not included in the test setup since the design ensures low di/dt values for the diodes in the half-bridge (diodes are integrated in the IGCT package). For the resonant/switching frequencies of interest, the rate of change of current was still the order of magnitude lower than the datasheet requirement, which confirmed the discussion from previous chapter.

5. Experimental Results

Two types of experimental measurements were performed, resonant pulse test and continuous resonant operation test. The first type was inspired by the typical double pulse test where a turn-on and turn-off behavior of the semiconductor can be observed without a risk of damage. The double pulse test is typically used to characterize the switches for hard-switching application. As the current shape through the switch is different in the LLC-SRC mode of operation, resonant pulse test was derived in order to characterize the IGCTs under low current turn-off conditions and quasi sinusoidal pre-flooding. Results are later applied for estimating the continuous working conditions, ensuring safe operation.

Information regarding the turn-off delay time was used to define proper dead-time for the half-bridge. Safe Operating Area (SOA) conformity was tested for different turn-off currents and peak resonant currents. Turn-off energy losses are estimated and later used to predict the junction temperature rise for the given switching frequency in continuous regime.

5.1 Resonant Pulse This test is performed in order to characterize the IGCT in the resonant mode of operation. It is required as this is not a typical application of this kind of semiconductor switch and datasheet values give typical parameters for hard-switching applications.

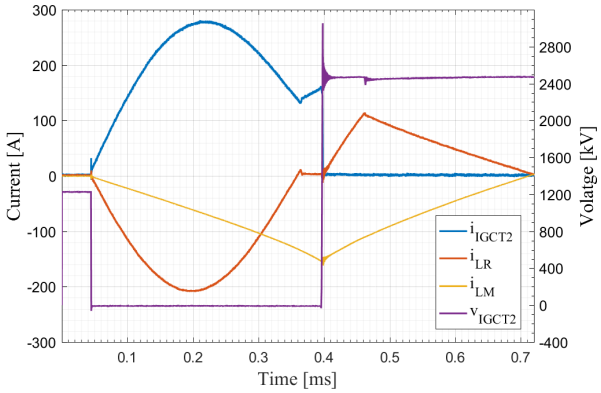

Fig. 7. One switch resonant pulse typical waveforms

Device under test is $IGCT_2$ from Fig. 6 and the typical test waveforms are shown in Fig. 7. The test is started by charging the DC-link to a predefined voltage level, 2.5 kV in this case. At this point $IGCT_1$ and $IGCT_2$ are blocking the DC-link and equally sharing the voltage among each other. At the same time, resonant capacitor voltage is charged to a predefined level, U_{C0}, depending on the desired peak resonant current for the particular test. Eq. (6) describes this dependency:

$$I_M = U_{C0}\sqrt{\frac{C_R}{L_R}} \quad \cdots\cdots (6)$$

where I_M is the amplitude of the resonant current, U_{CO} is the resonant capacitor pre-charge voltage for the desired I_M, C_R and L_R are resonant capacitance and inductance respectively.

$IGCT_2$ is then turned on, its voltage falls to zero and a current starts to build up. This current is the sum of the magnetization inductor (L_M) current and the resonant tank current i_{LR}. It should be noted that for this experiment, the high current source V_{DCR} is shorted out of the circuit.

Resonant current flows through the $IGCT_2$ and diode D_2 into the resonant capacitor, charging it in the opposite direction. When it falls to zero, the resonance is stopped and only the L_M current flows through the $IGCT_2$ which is later turned off at the moment corresponding to the predefined value of turn-off current. Turn-off current and voltage transient is recorded at this moment and the data is later used for the turn-off energy estimation - E_{off}, turn-off delay time measurement - t_{DOFF} and SOA conformity. The small spike in the resonant current waveform i_{LR} in Fig. 7, when it reaches zero, comes from the reverse recovery of the D_2 diode which turns off at this instant.

After the turn-off of the $IGCT_2$, no further external manipulation of the switches is performed. When the $IGCT_2$ turns off, i_{LM} commutates to the diode of the $IGCT_1$ and flows back to the DC-link (upper C_{DC} capacitor). Since this action lowers the voltage on the $IGCT_1$, diode D_1 becomes positively biased by C_R voltage (which is now negative) and starts conducting current originating from the resonant circuit i.e. new resonant cycle is started. The i_{LR} during the 0.4–0.46 ms period is the current in the resonant circuit only

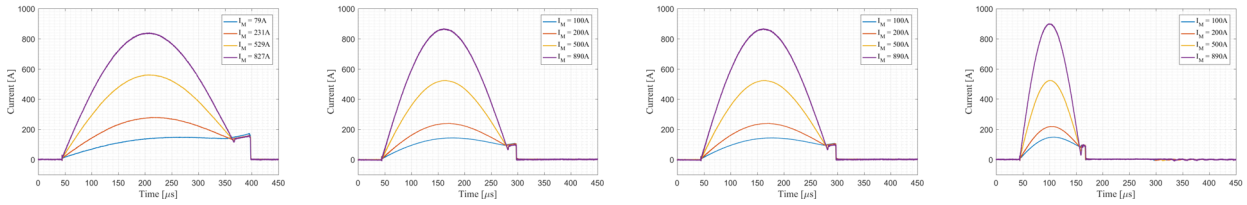

Fig. 8. Resonant pulses with constant turn-off current and frequency and variable resonant peak a) I_{off} = 160 A, f_{SW} = 1440 Hz b) I_{off} = 100 A, f_{SW} = 2000 Hz c) I_{off} = 130 A, f_{SW} = 3000 Hz d) I_{off} = 100 A, f_{SW} = 4000 Hz

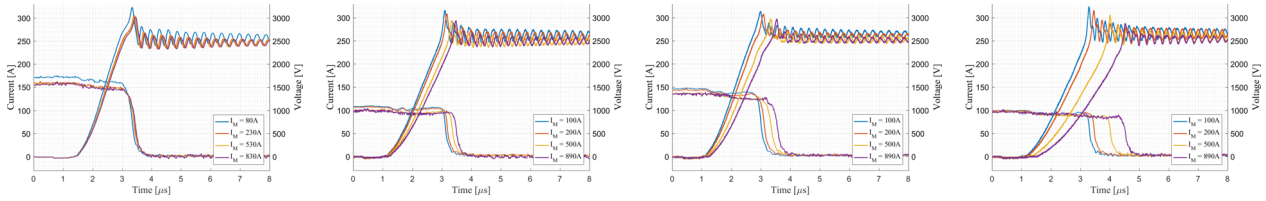

Fig. 9. Turn-off transients a) I_{off} = 160 A, f_{SW} = 1440 Hz b) I_{off} = 100 A, f_{SW} = 2000 Hz c) I_{off} = 130 A, f_{SW} = 3000 Hz d) I_{off} = 100 A, f_{SW} = 4000 Hz

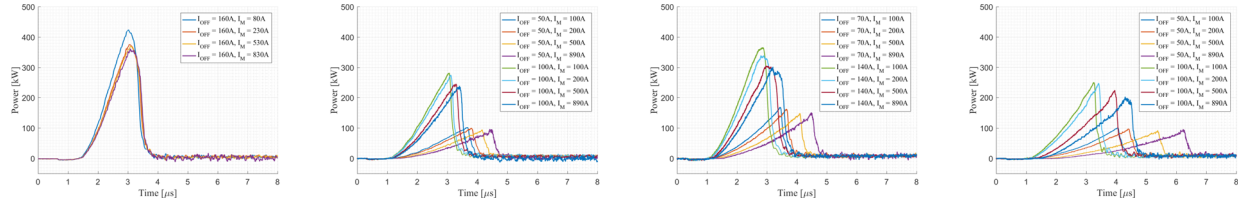

Fig. 10. Turn-off power transients a) I_{off} = 160 A, f_{SW} = 1440 Hz b) I_{off} = 100 A, f_{SW} = 2000 Hz c) I_{off} = 130 A, f_{SW} = 3000 Hz d) I_{off} = 100 A, f_{SW} = 4000 Hz

(i_{LM} flows through the diode of $IGCT_1$). At 0.46 ms moment, resonant current and i_{LM} become equal and i_{LM} commutates from $IGCT_1$ to resonant tank. Resonance is now stopped and i_{LM} falls to zero under the influence of the sum of the half of the DC-link and C_R voltage. C_R voltage, being negative (and much lover than the DC-link voltage), reverse biases the diode of the $IGCT_1$ and it stops conducting. After the 0.46 ms moment, i_{LM} and i_{LR} are equal in value and the current is fed back to the DC-link until it reaches zero.

The described test is performed for different low turn-off currents, switching and resonant frequencies as well as different resonant current peaks in order to observe particular influences on turn-off behavior of the IGCT. Characterization data is later used for defining the safe operating conditions for the continuous resonant operation test.

Figure 8 shows the $IGCT_2$ load current for the different resonant pulse tests. Switching and resonant frequency is varied throughout the experiment as well as the peak resonant current and turn-off current.

All of the tests are performed at 2.5 kV DC-link voltage and the 30°C water inlet temperature. As the pulses were short and time between two consecutive tests was much larger than the thermal constant of the IGCT, it is assumed that the junction temperature haven't risen significantly above the heatsink temperature. Consequently, the test data is valid for the 30°C junction temperature.

Figure 9 show the zoomed in turn-off transients. Turn-off current variations are kept as tight as possible for the particular set of waveforms and the small variations are due to the small variations in the DC-link voltage among the tests. In the Fig. 9(a) it can be noticed that the resonant peak value has no influence on the turn-off transient whatsoever. As the length of the pulse decreases for the further tests (equivalent for the increase in switching frequency), Figs. 9(b)–9(d), the influence starts becoming pronounced more and more. Storage time slightly prolongs and dV/dt gets lower as the peak resonant current increases. With a shorter pulses, the stored charge becomes dependent not only on a value of a current flow through the device but on its derivative as well. The effect increases as the pulse duration decreases and approaches the recombination time of the IGCT.

Transient power loss waveforms are obtained by multiplying the current and voltage for the particular turn-off transient and are presented in Fig. 10. Integration of these waveforms over time yields the turn-off energy lost per pulse - E_{off}, summarized in Fig. 12. The graph shows the turn-off energy as the function of turn-off current for different switching frequencies and peak resonant currents. Switching frequency and peak resonant current show no significant influence on the E_{off} but only the turn-off current. These results are later used for power loss junction temperature rise estimation of the IGCT half-bridge during the continuous operation.

5.2 Continuous Operation Turn-off delay time, t_{DOFF} is measured and presented in Fig. 11 as a function of the turn-off current. As already mentioned, peak resonant current prolongs the time needed for the IGCT to turn-off at short resonant pulses and this effect is best noticed at the 4 kHz equivalent operation pulses (blue dots in Fig. 11). As

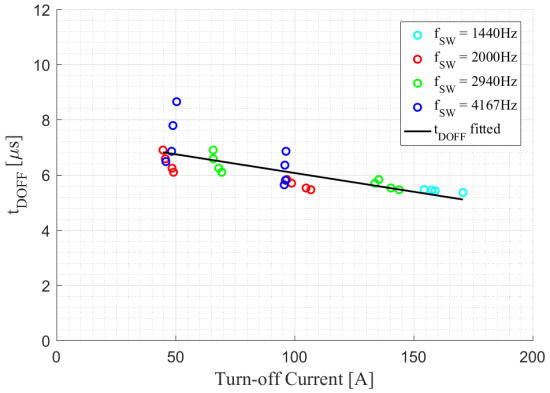

Fig. 11. Measured turn-off delay times for different turn-off currents and frequencies

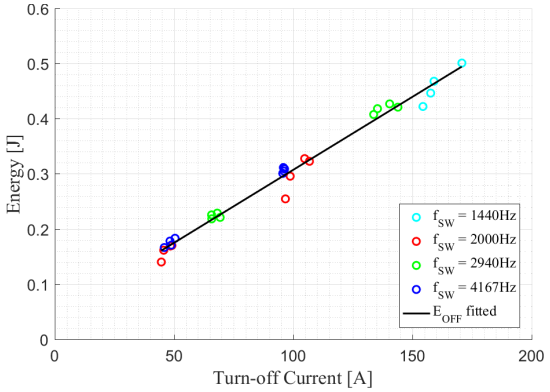

Fig. 12. Calculated turn-off energy losses for different turn-off currents and frequencies

the loading resonant current of the IGCT increases so does the t_{DOFF} and this has to be taken into account in the design phase of the LLC-SRC for proper dead-time selection. Another observation is that the variability of t_{DOFF} with peak resonant current decreases as the turn-off current increases and becomes more controllable at slightly higher turn-off currents. Finally, a trade off has to be made between the short and steady turn-off, meaning increase in I_{off}, and the turn-off energy losses which directly increase with the increase in turn-off current.

After the initial resonant pulse testing and with the successful acquisition of the baseline values for the t_{DOFF} and E_{off} parameters, the test setup was run in the continuous mode of operation. During this test, the high current DC source V_{DCR} from Fig. 6 was employed in the circuit to account for the losses during the energy transfer from C_R to L_R and vice versa. Table 2 summarizes different configurations of the test setup for different experiments performed.

Continuous switching at two different frequencies and different turn-off currents was tested. Table 3 shows the preliminary power loss calculation for the IGCTs and the anti-parallel diodes. Calculations and estimations are done using the following equations:

$$P_{CND} = V_{T0} I_T^{avg} + r_T (I_T^{rms})^2 \quad \cdots\cdots\cdots\cdots\cdots\cdots \quad (7)$$

$$P_{SW} = E_{OFF} f_{SW} \quad \cdots\cdots\cdots\cdots\cdots\cdots\cdots\cdots \quad (8)$$

where I_T^{avg} and I_T^{rms} are average and root-mean-square values of the IGCT current respectively, V_{T0} is a threshold voltage

Table 2. Continuous resonant operation test parameters for different experiments

Parameter	Experiment 1	Experiment 2	Experiment 3
$IGCT_1, IGCT_2$	5SHX 1445H		
D_1, D_2	5SDF 10H4503		
V_{DC} [V]	2x1250	2x1250	2x1250
C_{DC} [mF]	2.6	2.6	2.6
C_R [μF]	660	660	660
L_R [μH]	15	15	7.5
f_R [Hz]	1600	1600	2260
f_{SW} [Hz]	1440	1440	1860
L_M [mH]	3	1.5	1.5
I_{off} [A]	70	140	100
I_{rm} [A]	910	910	910
t_{DOFF} [μs]	3.4	2.9	3.1
t_{DCND} [μs]	7.6	14.5	8.1
t_D [μs]	8	15	8

Table 3. Estimation of the conduction and switching losses for the switching half-bridge

Parameter	Experiment 1	Experiment 2	Experiment 3
I_T^{avg} [A]	261	262	240
I_T^{rms} [A]	428	427	403
P_{CND}^T [W]	797	797	721
E_{OFF}^T [J]	0.16	0.33	0.23
P_{SW}^T [W]	230	475	428
I_D^{avg} [A]	0.4	1.5	0.8
I_D^{rms} [A]	4.4	12	8.0
P_{CND}^D [W]	1.0	4.4	2.3
P_{TOTAL} [kW]	2.1	2.6	2.3

and r_T is the slope resistance. E_{OFF} is the turn-off energy of the IGCT given for the specific turn-off current and f_{SW} is the switching frequency. Conduction losses of the free-wheeling diode are estimated as well, neglecting the reverse recovery losses; low di/dt during the turn-off justifies this assumption. As the calculation showed the numbers within the datasheet limits of the semiconductor devices, experiments were run to confirm the predicted operation of the test setup.

Experiments were run without any major or minor operation issues and the waveform data was collected. $IGCT_1$ and $IGCT_2$ continuous operation waveforms are presented in Fig. 13 for switching frequencies of 1440 Hz and 1860 Hz respectively. Slight deviations between the current waveforms of the two switches come from the non-symmetrical resonant current loops. Because of its size, the high current voltage source V_{DCR}, Fig. 6, is placed outside the test cabinet and connected into the circuit using relatively long cables. This connection introduces additional parasitic inductance into the circuit, roughly 2 μH, slightly changing the resonant tank parameters seen by the $IGCT_2$ switch.

Turn-off current of the IGCTs was kept constant among the different experimental runs and clamp-less operation of the IGCTs achieved. Rate of change of the current in the diodes in the LLC-SRC bridge is naturally limited by the resonant tank and makes the clamp circuit redundant in this application. Its removal has a positive impact on the power density of the future IGCT based DC-DC converter designs. One pos-

sible drawback of the clamp inductor removal is short circuit current limitation. If the half-bridge should short circuit, only the parasitic inductance of the bus-bars would limit the current allowing for the much higher values of the short circuit current to arise.

Detailed turn-off transients are presented in Fig. 14, showing the current and voltage waveforms of the $IGCT_2$ for different switching frequencies, turn-off currents and peak resonant currents. All the signals are synchronized in time, with zero on the time axis representing the moment when the optical signal ant the IGCT's control input goes low. The turn-off signal itself is not shown for clarity purposes.

First thing that can be noticed in the waveforms is that the turn-off delay time, t_{DOFF} varies with the load current. The t_{DOFF} parameter is summarized with the plot in Fig. 15 with values measured from all of the waveforms from the three experiments. This finding could lead to a conclusion that the t_{DOFF} is a function of the maximum resonant (load) current through the device only but there is a lurking variable present here: the IGCT junction temperature. It must be noted that the temperature of the junction was not controlled during the experiments; cooling inlet water temperature was kept at the 30°C, as this was the only controllable temperature in the system. It was shown in the previous work [24], through simulation and experiment, that t_{DOFF} mostly depends on the junction temperature and the value of the turn-off current of the IGCT when the blocking voltage is kept constant (2.5 kV in this case). The relatively high variability of t_{DOFF} in continuous operation (Fig. 15), compared to low variability seen in Fig. 11, is caused by the different operating junction temperature of the IGCT at the different loading conditions.

As the power losses of the IGCT vary significantly with the maximum of the resonant current, the prolongation of the t_{DOFF} is accounted to the change in temperature of the semiconductor junction. With a test setup running in a continuous regime and relatively low thermal junction-to-heatsink constant of the IGCT, the waveform triplets represent the samples at a working temperature corresponding to the given load at the moment of the recording of the waveforms. The higher the load current, the higher the working temperature of the IGCT that influences the t_{DOFF} parameter by increasing its duration.

The similar explanation holds the turn-off energy losses depicted in the Fig. 16, estimated by the time integration of the product of the IGCT's current and voltage waveforms during the turn-off period. The delays originating from the current and voltage measurement methods (probe delays, cable propagation delays) were already accounted for by setting the respective deskew delays on the measuring channels of the oscilloscope. Proper aligning of the current and voltage waveforms is essential for this method of the turn-off losses evaluation.

Comparing the results in Fig. 12 and Fig. 16, it can be seen that the turn-off energy losses are higher in the later figure. This result is expected as the Fig. 12 summarizes the resonant pulse test results at the junction temperature of 30°C while

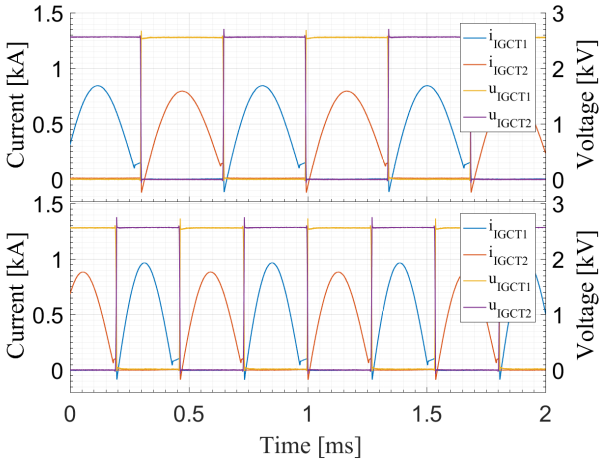

Fig. 13. Experimental waveforms (voltage and current) for the continuous operation of the $IGCT_1$ and $IGCT_2$ under the resonant operating conditions: top f_{SW} = 1440 Hz, bottom f_{SW} = 1860 Hz

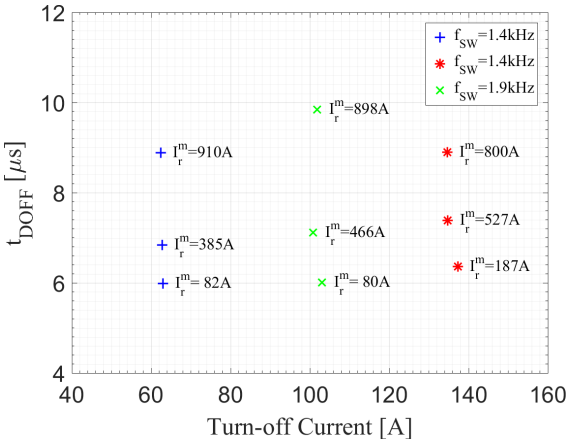

Fig. 15. Turn-off delay time estimated from the experimental current and voltage waveforms

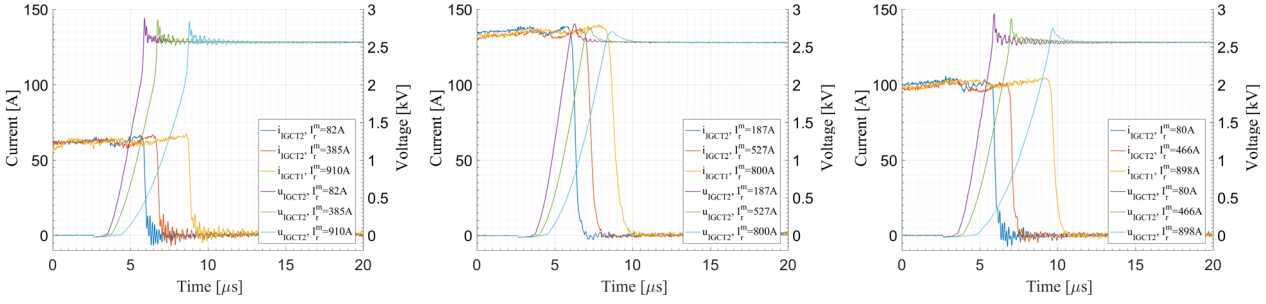

Fig. 14. Turn-off current and voltage waveforms a) f_{SW} = 1440 Hz, I_{OFF} = 70 A b) f_{SW} = 1440 Hz, I_{OFF} = 140 A c) f_{SW} = 1860 Hz, I_{OFF} = 100 A

o

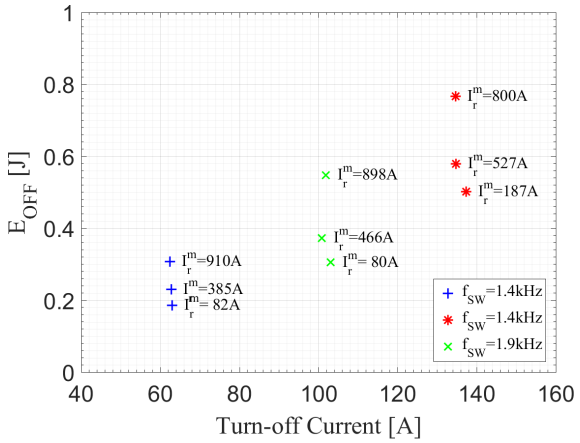

Fig. 16. Estimated turn-off energy losses

Fig. 16 shows the results under the continuous load conditions that directly influence the junction temperature of the IGCT.

Comparing the values in Fig. 16 and the estimations done before running the experiments from Table 3, it can be noted that the IGCT switching losses become a considerable portion of the total losses of LLC-SRC half-bridge. In order to have even higher switching frequencies of the converter, switching losses have to be lowered, either by lowering the turn-off current or by choosing an IGCT device optimized for switching rather than conduction losses. Allowing for the higher temperature rise of the semiconductor by lowering the thermal conductivity of the case is another solution but this one comes at the cost of lower efficiency of the converter.

Another issue noticed in the turn-off waveforms in Fig. 14(a) and Fig. 14(c) is rather oscillatory turn-off of the IGCT. The response can be improved by lowering the parasitic inductance of the DC-link bus-bars connecting the half-bridge and the DC-link in order to provide better attenuation of the system. If the decrease of the parasitic inductance of this commutation loop is not possible, the turn-off current of the IGCT has to be increased to counteract the ringing, since these oscillations could cause the electromagnetic interference problems and the additional losses.

6. Conclusions

Basic challenges of implementing an IGCT in a LLC-SRC soft switching topology are outlined in this paper. High frequency operation and low switching losses are two opposing requirements closely tied to the turn-off current of the switch dictating the turn-off speed and dead-time selection. The designer of such a topology has to make a trade off based on the application of the converter unit.

Successful application of the IGCT was demonstrated through the experiment in the test setup providing LLC-SRC current/voltage stress environment for the semiconductor switch. Relatively high switching frequency of the IGCT was achieved when compared to the typical hard-switching application (up to 900 Hz). Clamp-less operation was successful with no additional stress on the diodes, which proved the theoretical assumptions that LLC-SRC does not require the clamp circuit.

Estimation of the turn-off delay time parameter and turn-off losses using a resonant-pulse data proved to be useful as the first step during the design process of the converter. High temperature test data would be more insightful for the final design and is going to be examined for the future works by the authors. Measuring the parameters on the test setup working in continuous mode of operation gave the further insight into temperature influence of the turn-off behavior and the lessons learned pave way for reaching even higher operation frequencies.

Acknowledgment

The work presented in the paper is supported in part by the Swiss National Science Foundation under the project number 200021_165566 and in part by ABB Semiconductors, Lenzburg, Switzerland.

References

(1) D. Dujic, F. Kieferndorf, F. Canales, and U. Drofenik: “Power electronic traction transformer technology”, Power Electronics and Motion Control Conference (IPEMC), 2012 7th International, Vol.1, pp.636–642 (2012)

(2) Z. Chen, Z. Yu, X. Zhang, T. Wei, G. Lyu, L. Qu, Y. Huang, and R. Zeng: “Analysis and Experiments for IGBT, IEGT, and IGCT in Hybrid DC Circuit Breaker”, *IEEE Transactions on Industrial Electronics*, Vol.65, No.4, pp.2883–2892 (2018)

(3) D. Dujic, S. Lewdeni-Schmid, A. Mester, C. Zhao, M. Weiss, J. Steinke, M. Pellerin, and T. Chaudhuri: “Experimental characterization of LLC resonant DC/DC converter for medium voltage applications”, Proceedings of the PCIM Europe 2011, pp.265–271 (2011)

(4) H.A.B. Siddique and R.W. De Doncker: “Evaluation of DC Collector-Grid Configurations for Large Photovoltaic Parks”, *IEEE Transactions on Power Delivery*, Vol.33, No.1, pp.311–320 (2018)

(5) S. Milovanovic and D. Dujic: “MMC-Based High Power DC-DC Converter Employing Scott Transformer”, PCIM Europe 2018 International Exhibition and Conference for Power Electronics, Intelligent Motion, Renewable Energy and Energy Management (2018)

(6) U. Javaid, D. Dujic, and W. van der Merwe: “MVDC marine electrical distribution: Are we ready?”, IECON 2015 - 41st Annual Conference of the IEEE Industrial Electronics Society, pp.823–828 (2015)

(7) S. Castellan, R. Menis, A. Tessarolo, and G. Sulligoi: “Power electronics for all-electric ships with MVDC power distribution system: An overview”, 2014 Ninth International Conference on Ecological Vehicles and Renewable Energies (EVER), pp.1–7 (2014)

(8) U. Javaid, F.D. Freijedo, D. Dujic, and W. van der Merwe: “MVDC supply technologies for marine electrical distribution systems”, *CPSS Transactions on Power Electronics and Applications*, Vol.3, No.1, pp.65–76 (2018)

(9) C. Dincan, P. Kjaer, Y. Chen, S. Nielsen, and C. L. Bak: “Selection of DC/DC converter for offshore wind farms with MVDC power collection”, 2017 19th European Conference on Power Electronics and Applications (EPE’17 ECCE Europe), pp.1–10 (2017)

(10) J. Robinson, D. Jovcic, and G. Joos: “Analysis and Design of an Offshore Wind Farm Using a MVDC Grid”, *IEEE Transactions on Power Delivery*, Vol.25, No.4, pp.2164–2173 (2010)

(11) N. Soltau, H. Stagge, R.W. De Doncker, and O. Apeldoorn: “Development and demonstration of a medium-voltage high-power DC-DC converter for DC distribution systems”, 2014 IEEE 5th International Symposium on Power Electronics for Distributed Generation Systems (PEDG), pp.1–8 (2014)

(12) M. Stieneker and R.W. De Doncker: “Dual-active bridge DC-DC converter systems for medium-voltage DC distribution grids”, 2015 IEEE 13th Brazilian Power Electronics Conference and 1st Southern Power Electronics Conference (COBEP/SPEC), pp.1–6 (2015)

(13) C. Meyer and R.W. De Doncker: “Design of a Three-Phase Series Resonant Converter for Offshore DC Grids”, 2007 IEEE Industry Applications Annual Meeting, pp.216–223 (2007)

(14) C. Dincan, P. Kjaer, Y. Chen, S. Munk-Nielsen, and C.L. Bak: “Analysis of a High-Power, Resonant DC-DC Converter for DC Wind Turbines”, *IEEE Transactions on Power Electronics*, Vol.33, No.9, pp.7438–7454 (2018)

(15) P. Steimer, H.E. Gruning, J. Werninger, E. Carroll, S. Klaka, and S. Linder: “IGCT - a new emerging technology for high power, low cost inverters”, *IEEE Industry Applications Magazine*, Vol.5, No.4, pp.12–18 (1999)

(16) U. Vemulapati, M. Rahimo, M. Arnold, T. Wikström, J. Vobecky, B. Backlund, and T. Stiasny: “Recent advancements in IGCT technologies

for high power electronics applications", Power Electronics and Applications (EPE'15 ECCE-Europe), 2015 17th European Conference on, pp.1–10 (2015)
(17) B. Zhao, R. Zeng, Z. Yu, Q. Song, Y. Huang, Z. Chen, and T. Wei: "A More Prospective Look at IGCT: Uncovering a Promising Choice for DC Grids", *IEEE Industrial Electronics Magazine*, Vol.12, No.3, pp.6–18 (2018)
(18) P. Ladoux, N. Serbia, and E.I. Carroll: "On the Potential of IGCTs in HVDC", *IEEE Journal of Emerging and Selected Topics in Power Electronics*, Vol.3, No.3, pp.780–793 (2015)
(19) F. Filsecker, R. Alvarez, and S. Bernet: "Comparison of 4.5 kV Press-Pack IGBTs and IGCTs for Medium-Voltage Converters", *IEEE Transactions on Industrial Electronics*, Vol.60, No.2, pp.440–449 (2013)
(20) R. Alvarez, F. Filsecker, M. Buschendorf, and S. Bernet: "Characterization of 4.5 kV/2.4 kA press pack IGBT including comparison with IGCT", 2013 IEEE Energy Conversion Congress and Exposition, pp.260–267 (2013)
(21) ABB Semiconductors, online: https://new.abb.com/semiconductors/integrated-gate-commutated-thyristors-(igct)
(22) Toshiba Electronics Devices & Storage Corporation, online: https://toshiba.semicon-storage.com/eu/product/igbt-iegt/iegt/ppi.html
(23) T. Duerbaum: "First harmonic approximation including design constraints", INTELEC - Twentieth International Telecommunications Energy Conference (Cat. No.98CH36263), pp.321–328 (1998)
(24) D. Stamenkovic, D. Dujic, M. Rahimo, U. Vemulapati, and T. Stiasny: "IGCT Switching Behaviour Under Resonant Operating Conditions", 2018 20th European Conference on Power Electronics and Applications (EPE'18 ECCE Europe), pp.1–9 (2018)

Dragan Stamenkovic (Non-member) received his Dipl.Ing. (2008) and M.Sc. (2010) degrees in electrical engineering from the University of Belgrade, Serbia. In 2011, he joined GE Global Research, Munich as a power electronics development engineer with focus on wind turbine converters and later continued his career with GE Power Conversion, Berlin in the area of medium voltage drives. Currently, he is pursuing the Ph.D. degree at Power Electronics Laboratory at EPFL, Lausanne, Switzerland, with the main focus on high power converters for MVDC applications.

Drazen Dujic (Non-member) received the Dipl.-Ing. and M.Sc. degrees from the University of Novi Sad, Novi Sad, Serbia, in 2002 and 2005, respectively, and the Ph.D. degree from the Liverpool John Moores University, Liverpool, U.K., in 2008. From 2002 to 2006, he was with the Department of Electrical Engineering, University of Novi Sad as a Research Assistant, and from 2006 to 2009 with Liverpool John Moores University as a Research Associate. From 2009 till 2013, he was with ABB Corporate Research Centre, Switzerland as a Principal Scientist working on the power electronics projects spanning the range from low-voltage/power SMPS in below kilowatt range to medium voltage high-power converters in a megawatt range. From 2013 till 2014, he was with ABB Medium Voltage Drives, Turgi, Switzerland, as R&D Platform Manager. He is currently with Ecole Polytechnique Federale de Lausanne EPFL, Lausanne, Switzerland, as an Assistant Professor and the Director of the Power Electronics Laboratory. His current research interests include the areas of design and control of advanced high-power medium-voltage power electronics conversion systems and applications. He has authored or coauthored more than 100 scientific publications and has filed twelve patents. He is an Associate Editor for IEEE Transactions on Industrial Electronics, IEEE Transaction on Power Electronics and IET Electric Power Applications. In 2018 he has received EPE Outstanding Service Award and in 2014, the Isao Takahashi Power Electronics Award for outstanding achievement in power electronics.